Multiple charge-density-wave transitions in single-crystalline $Lu_2Ir_3Si_5$

N. S. Sangeetha,[1,*] A. Thamizhavel,[1] C. V. Tomy,[2] Saurabh Basu,[3] A. M. Awasthi,[4] Piu Rajak,[1] Somnath Bhattacharyya,[1] S. Ramakrishnan,[1,†] and D. Pal[3,‡]

[1]*Department of Condensed Matter Physics and Materials Science, Tata Institute of Fundamental Research, Homi Bhabha Road, Colaba, Mumbai-400 005, India*

[2]*Department of Physics, Indian Institute of Technology Bombay, Mumbai-400076, India*

[3]*Department of Physics, Indian Institute of Technology Guwahati, Guwahati, Assam-781039, India*

[4]*UGC-DAE Consortium for Scientific Research, University Campus, Khandwa Road, Indore-452 001, India*

(Received 14 October 2013; revised manuscript received 5 May 2015; published 26 May 2015)

The physical properties of the single-crystalline samples of $Lu_2Ir_3Si_5$ have been investigated by magnetic susceptibility, resistivity, and heat capacity studies. We observed multiple charge-density-wave (CDW) transitions in all the measurements. A strong thermal hysteresis at these transitions suggests a possible first order CDW ordering. In addition, the first order nature is ascertained by a very narrow and a huge cusp (62 J/mol K) in the zero field specific heat data which also suggests strong electron-phonon interchain coupling.

DOI: 10.1103/PhysRevB.91.205131 PACS number(s): 71.45.Lr, 71.20.Eh

I. INTRODUCTION

Charge-density-wave (CDW) transitions are expected to occur in low-dimensional solids, where it is possible to achieve nesting of Fermi surfaces that lead to the appearance of a periodic lattice distortion with an accompanying energy gap. The possibility of such an instability to arise in low-dimensional solids was first theoretically demonstrated by Peierls [1,2]. This is very well documented from the early works of many research groups who performed studies on a wide range of quasi-low-dimensional systems which include transition-metal dichalcogenides and trichalcogenides [3–6]. Though it is not possible to get a perfect nesting in three-dimensional (3D) compounds, CDW ordering has been reported in 3D materials such as $R_2Ir_3Si_5$ [7] and $R_5Ir_4Si_{10}$ [8] (R = rare-earth elements). This establishes that even in the absence of perfect nesting, there remains a possibility for the appearance of a CDW. In order to understand the nature of such novel CDW in 3D systems, further searches for new classes of materials are needed.

Recently reported $R_5Ir_4Si_{10}$ (R = Dy-Lu) compounds exhibit strong electron-phonon coupling CDW at high temperatures, accompanied by superconductivity or magnetic ordering at low temperature [9]. Interestingly, multiple CDW anomalies were observed in $R_5Ir_4Si_{10}$ series (R = Dy, Ho, Er, and Tm) [10]. Among which, $Lu_5Ir_4Si_{10}$ shows the coexistence of superconductivity and strongly coupled CDW transition [11]. It has been reported that the compound $R_5Ir_4Si_{10}$ presents a complex 3D structure with several substructures such as one-dimensional R chains and 3D cages in which a variety of many-body effects (superconductivity and magnetism) could originate. Recently, the notion is that the phase transitions in complex systems can happen through several unconventional intermediate states and it has been supported by the observation of the quantum critical phenomena in 2H-$NbSe_2$ [12] and the evidence for a Peierls transition in TaS_2 [13], which are 2D conventional CDW systems. Interestingly, Mansart *et al.* [14] have reported, very recently, the melting of CDW and its consequent redistribution of charge carriers by ultrafast experiments in a complex 3D-solid $Lu_5Ir_4Si_{10}$. In addition, this experiment contributes an exciting and current debate by showing evidence of a Peierls transition in a 3D system.

The rare-earth ternary silicides $R_2Ir_3Si_5$ system has also received current research attention owing to its complex 3D crystal structure and the unusual ground states that they exhibit, such as superconductivity, CDW, Kondo behavior, coexistence of CDW and superconductivity or magnetism, etc. [7]. In this series, the compound $Lu_2Ir_3Si_5$ is of special interest, as it exhibits superconductivity at 3.5 K and shows strongly coupled (electron phonon) first order CDW transition between 150 and 200 K [15]. Recently, Kuo *et al.* [16] have reconfirmed the possibility for the CDW transition accompanying a similar structural phase transition from taking transport measurements. Later, Lee *et al.* have confirmed the CDW state in a $Lu_2Ir_3Si_5$ system via the presence of superlattice reflections with a wave vector $q = \delta(\bar{1}21)$, $\delta = 0.23$–0.25, adopted from the transmission electron microscopy (TEM) measurements on some selected single crystal grains separated from the polycrystalline melt [17]. In addition to the CDW superlattice spots, forbidden Bragg reflections ($h0l$), which violate the extinction condition of $h, l = 2n$, such as ($\bar{1}01$), ($\bar{3}03$), and so on, signify the structural transition associated with the CDW transition. Though the TEM studies were performed on small grains of polycrystalline sample, it can be treated as a single crystal since the selected area's electron diffraction pattern can be obtained from a much smaller area. Furthermore, in our earlier work, we have reported a nonmonotonicity of the transition temperatures T_{CDW} and T_{SC} as a function of Ge substitution [18]. This study reveals the complex nature of the CDW ordering such that the system may undergo coexistence of different phases with the suppression of CDW up to certain Ge concentrations, and afterwards, a sudden enhancement of it. Definite understanding of this scenario needs further

*nssangeetha@ameslab.gov; current address: Ames Laboratory and Department of Physics and Astronomy, Iowa State University, Ames, Iowa 50011, USA.

†ramky@tifr.res.in

‡dpal@iitg.ernet.in

experimentation on high quality single crystals of $Lu_2Ir_3Si_5$. In this paper we report an observation of multiple CDW transitions in a $Lu_2Ir_3Si_5$ single crystal using thermodynamic, transport, and magnetic measurements.

II. EXPERIMENT

Single-crystalline samples were grown in a tetra-arc furnace using a modified Czochralski technique. The purity of the elements is Lu: 99.99%; Ir: 99.99%; Si: 99.999%. The stoichiometric ratios of elements were taken separately to make a 12 g (polycrystal) melt in a tetra-arc furnace. A thin tungsten seed rod was immersed into the melt and pulled at a speed of 11 mm/h in a pure, dry argon atmosphere. After confirming the phase homogeneity of the grown crystal by using powder x-ray diffraction, the first grown crystal rod was then used as a seed in order to synthesize good quality single crystals of $Lu_2Ir_3Si_5$. Parts of the single crystals were sealed in a quartz tube and annealed under high vacuum at 900 °C for about 15 days.

The homogeneity of the compound $Lu_2Ir_3Si_5$ was checked on a polished surface of the sample by using EDAX and the amount of secondary phase was found to be less than 1%. Powder x-ray diffraction with Cu $K\alpha$ radiation was taken on the samples at 300 K by using an PANalytical commercial x-ray diffractometer. A commercial superconducting quantum interference device (SQUID) magnetometer (MPMS5, Quantum Design, USA) was used to measure dc magnetic susceptibility as a function of temperature between 100 and 300 K. The electrical resistivity between 1.8 and 300 K was measured by using a home built electrical resistivity set up with the standard dc four probe technique. The specific heat data were taken by using a DSC setup and a commercial physical property measurement system (PPMS, Quantum Design, USA). The reproducibility of the results was checked by repeating the measurements several times on the same samples.

III. RESULTS

A. X-ray diffraction studies

The powder x-ray diffraction pattern of $Lu_2Ir_3Si_5$ at 300 K clearly reveals the absence of any impurity phase and also confirms that the samples have a $U_2Co_3Si_5$-orthorhombic type structure with the space group $Ibam$. The Fullprof Rietveld fit [19] to the powder x-ray data of $Lu_2Ir_3Si_5$ is shown in Fig. 1. The extracted lattice parameters from this fit are $a = 9.923 \pm 0.0005$ Å, $b = 11.311 \pm 0.0005$ Å, and $c = 5.732 \pm 0.0005$ Å which are in close agreement with the previously reported polycrystalline data $a = 9.915$ Å, $b = 11.287$ Å, and $c = 5.722$ Å [15].

The single-crystalline nature of the samples was verified by using the back-reflection Laue diffraction technique. These single crystals were found to be oriented along three principal, mutually perpendicular, crystallographic directions. The observed Laue pattern of each direction was analyzed, with the simulated pattern, by using the Orient Express software. The observed Laue pattern of an oriented crystal, along [100] direction, is shown in Fig. 2. For transport and magnetization

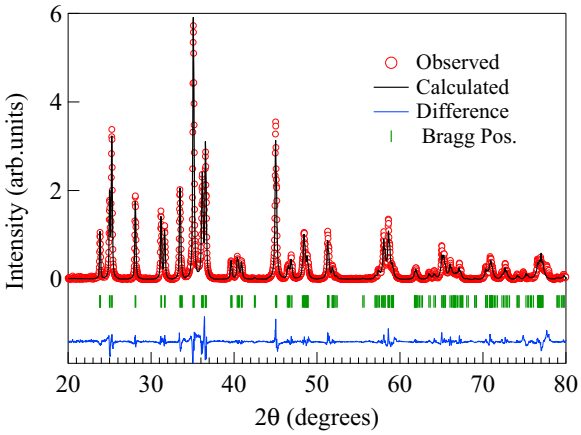

FIG. 1. (Color online) Powder x-ray diffraction data of the $Lu_2Ir_3Si_5$ at 300 K. The solid line is the simulated data using the FullProf (Rietveld program).

measurements, small bars (required size) were cut from the oriented single crystals by using a spark erosion technique.

Figure 3 depicts the unit cell of a $Lu_2Ir_3Si_5$ crystal structure. The Ir-Si-Ir bond is formed as a cage around the Lu atom which is stacked along the *ab* plane, shown in Fig. 3(a). The Lu atoms form a quasi-one-dimensional (1D) zigzag chain along the *c* axis [Fig. 3(a)] which are well separated from the Ir-Si ring. It can be found, in Fig. 3(b), that the zigzag chain of Lu atoms is strongly coupled with the *b* axis through the Ir1 atom. By analyzing the distances between other atoms, these Lu atoms have the shortest distance with respect to all other bonds; suggesting a quasi-1D conducting channel in the Lu-Lu chain, developing along the *c* axis.

B. *In situ* cooling TEM study of $Lu_2Ir_3Si_5$ single crystal

For TEM sample preparation, a piece of the single crystal was placed in a 1.2 mm × 1.8 mm slot of a titanium 3 slots grid and fixed with G1 epoxy. Then grinding and dimpling were done to bring down the specimen thickness to a residual value of 10 to 15 μm, and finally Ar+ ion-beam thinning

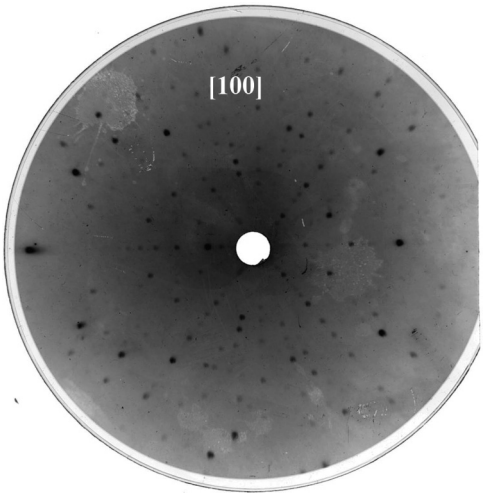

FIG. 2. The observed Laue pattern of $Lu_2Ir_3Si_5$ along [100] axis.

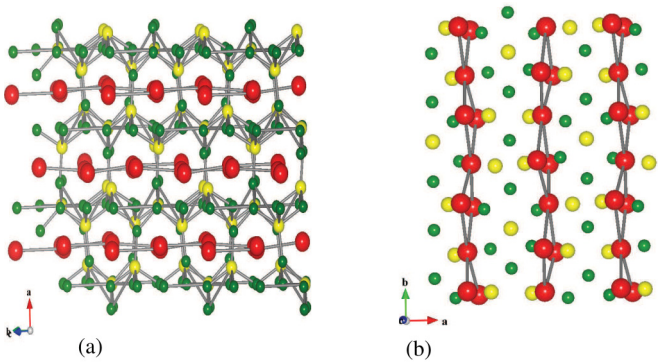

FIG. 3. (Color online) The crystal structure of $Lu_2Ir_3Si_5$. The large (red) spheres correspond to Lu atoms, Ir atoms with medium (yellow) spheres, and Si atoms with small (green) spheres.

was performed. By means of double-sided ion-beam etching at small angles (<6°) and low energies (acceleration voltage: 2.5 kV; beam current <8 μA), the introduction of artifacts was avoided. TEM experiments on single crystals were performed using a FEI-Tecnai microscope equipped with a LaB6 filament at an operating voltage of 200 kV [20]. All experimental data were collected when the specimen was oriented at [100] zone axis. All selected area diffraction patterns were collected from an area of 0.5 nm^2 on the sample, recorded on a 1 K × 1 K slow scan CCD camera and analyzed using the Digital Micrograph software (Gatan Inc., USA). *In situ* cooling TEM experiment was performed using a double tilt liquid N_2 cooling TEM specimen holder (Gatan Inc., USA), which is capable of reaching up to 100 K. Slow cooling of the sample inside the TEM was done, and, to achieve equilibrium, a substantially long waiting time of 4 h at 100 K in the absence of an electron beam was given before performing experiment.

Figures 4(a) and 4(b) show the selected area diffraction patterns (SADP) at room temperature and at 100 K, respectively. The measured distance between the diffraction spot (000) and (002) for the room temperature data, shown in Fig. 4(a), is 3.56 nm^{-1}. It corresponds to the d spacing of 0.28 nm and is denoted as d_1. The distance between the diffraction spots (020) and (022) is also the same (3.56 nm^{-1}) and is denoted as **A**. Similarly, the distance between the diffraction spots (000) and (020) is 1.84 nm^{-1}, which corresponds to the d spacing 0.54 nm, is denoted as d_2. The diffraction spots (020) and (040) are also similar (1.84 nm^{-1}) which is denoted as **B**. In order to protect the CCD from the intense (000) spot, we used a spot stopper. As a result, (000) is not present in Fig. 4(b). The distances **A** and **B** at 100 K, shown in Fig. 4(b), are 6.31 and 7.57 nm^{-1}, respectively, which is different than that of the room temperature diffraction data. This diffraction pattern (with these distances) does not match with any possible zone axis orientation of the structure of $Lu_2Ir_3Si_5$. It should also be noted that spot splitting is observed in almost all diffraction spots, which is associated with the CDW phase transition below 150 K. Even the most intense spot has the same behavior, which is revealed from the 3D intensity distribution plot presented in Fig. 4(c) in the region indicated by the dotted box in Fig. 4(b). From the measured values of **A** and **B** in Fig. 4(b), we can calculate a new d_1 and d_2, which are both found to be 0.16 and 0.13 nm, respectively. Also, we have calculated the new lattice parameters b and c from the calculated d spacing to be 0.26 and 0.32 nm, respectively. These lattice constants are much smaller than the room temperature lattice parameters b (=1.08 nm) and c (=0.56 nm) values. However, it should be noted that in cooling data, at 100 K [Fig. 4(b)], the angle between **A** and **B** is 90° which means the direction [010] is perpendicular to [001], which is similar to the room temperature structure. We will return to this point later in the discussion section.

C. Electrical resistivity

Figure 5 shows the temperature dependence of resistivity of $Lu_2Ir_3Si_5$ along a, b, and c axes. In this figure, the inset of the left panel shows $\rho(T)$ on cooling and heating the sample in the temperature range of 140 and 300 K at the rate of 1 K/min. One can see from the figure that $\rho(T)$ exhibits a sharp upturn between 170 and 250 K on cooling and warming data. It signifies the opening up of a gap in the electronic density of states at the Fermi surface (FS). This behavior is similar to the one usually observed in charge-density-wave (CDW) transition. Another interesting feature observed in the resistivity plot is that there is a large hysteresis, of almost 40–50 K, between the up and down scans. This strongly suggests a first order CDW transition for the system. Besides, such a broad curvature and an unusually large upward jump seen in the resistivity data, with a steplike increase (on decreasing temperature) across the transition, clearly reveals the mixture

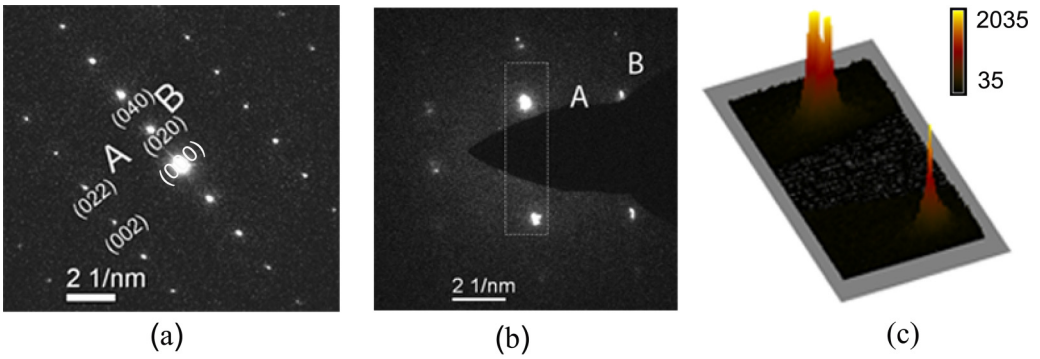

FIG. 4. (Color online) The selected area diffraction pattern (SADP) of $Lu_2Ir_3Si_5$ along [100] axis (a) at room temperature and (b) 100 K. (c) The 3D intensity distribution plot of the region indicated by the dotted box in (b).

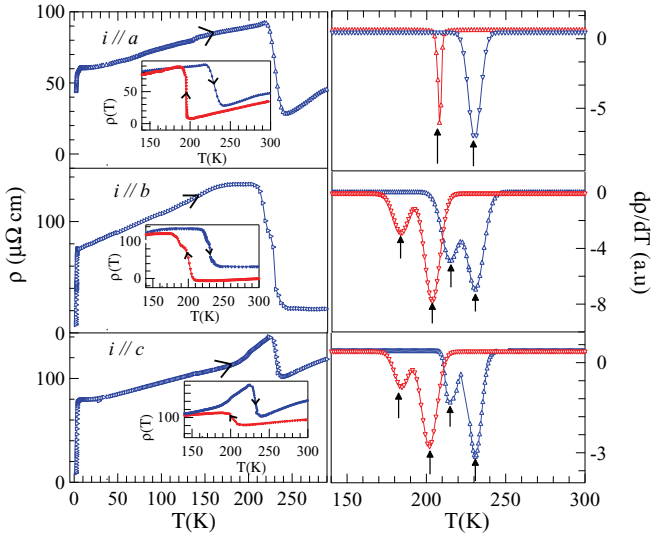

FIG. 5. (Color online) The temperature dependence of the electrical resistivity $\rho(T)$ of $Lu_2Ir_3Si_5$. Left panel shows the resistivity for temperature scans between 1.8 and 300 K. The inset of the left panel shows $\rho(T)$ illustrating the hysteresis between 140 and 300 K in the resistivity taken on the cooling (red triangle) and warming (blue triangle) cycle for $Lu_2Ir_3Si_5$ along the *a, b*, and *c* axes. Right panel shows $d\rho/dT$ as a function of temperature between 140 and 300 K highlighting multiple anomalies. The solid arrows indicate the transition temperatures of the anomalies.

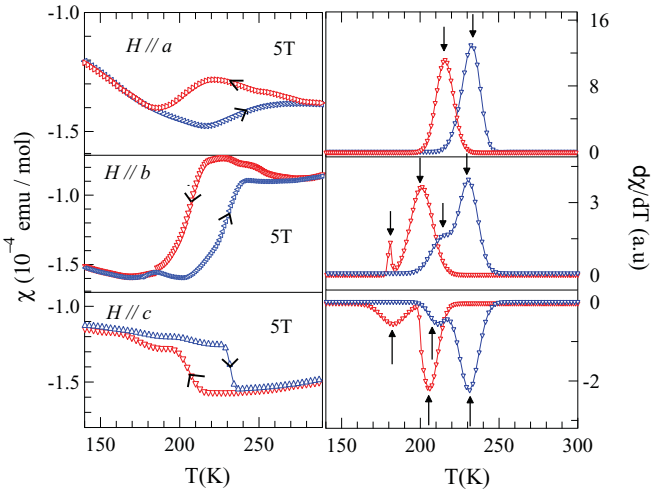

FIG. 6. (Color online) The temperature dependence of the dc susceptibility $\chi(T)$ of $Lu_2Ir_3Si_5$. Left panel demonstrates dc susceptibility in the temperature range between 140 and 300 K to highlight CDW transition along three principle axes (*a*, *b*, and *c*) for both cooling (red triangle) and warming (blue triangle) the sample, its corresponding derivative plots are shown in the right panel of the figure.

of multiple CDW phase in the sample (seen in Fig. 5) as were observed in $Er_5Ir_4Si_{10}$ [21].

In order to have a better understanding of CDW transitions, the derivative of resistivity ($d\rho/dT$ vs T) is also plotted against temperature (shown in right panel of Fig. 5). From this, one can clearly elucidate the presence of multiple transitions for cooling and warming the sample along *b* and *c* axes. These anomalies are marked with solid arrows. It must be noted that there is no second anomaly along the *a* axis. We shall return to this point as we discuss further. The characteristic CDW transition temperatures T_{CDW} obtained from resistivity measurement is listed in Table I.

D. Magnetic susceptibility

Figure 6 shows dc magnetic susceptibility and its derivative of $Lu_2Ir_3Si_5$ as a function of temperature from 150 to 300 K with an applied magnetic field $H = 5$ T along *a*, *b*, and *c* axes. The magnetic susceptibility data (shown in the left panel) show a large diamagnetic drop across the phase transition at around 250 and 170 K on warming and cooling the sample, respectively. This results in a reduction in the density of states at the FS due to the opening up of a gap at the FS accompanying the CDW ordering. A huge thermal hysteresis (40–50 K) associated with the CDW ordering along the three axes signifies a first order characteristic of CDW transition as observed in the resistivity results. The derivative plots of susceptibility ($d\chi/dT$ vs T), shown in the right panel of Fig. 6, demonstrate multiple CDW anomalies for *b* and *c* axes and are marked by solid arrows. The broad anomalies of susceptibility data also corroborate the above inference. Concurrently, one can see a single peak along the *a* axis as found in resistivity data. In contrast, there is an enhancement of magnetization across the CDW transition along the *c* axis. We shall discuss this later in the Discussion. The CDW transition temperature obtained from the susceptibility studies, listed in Table I, are in good agreement with the above mentioned resistivity results.

TABLE I. CDW transition temperatures T_{CDW} observed from both resistivity and susceptibility measurement techniques.

	Resistivity T_{CDW} (K)		Susceptibility T_{CDW} (K)	
Axis	Cooling	Warming	Cooling	Warming
a	197	231	199	232
	184	213	181	214
b	200	232	201	231
c	184	215	183	212
	202	231	204	230

E. Heat capacity

Figure 7 shows the zero field specific heat data, for $Lu_2Ir_3Si_5$, in the temperature range between 150 and 300 K. The lattice background subtraction is done by assuming Debye lattice, fitted by Einstein's model $C_L = a_1(\frac{a_2}{T})^{a_3}\frac{e^{a_1/T}}{(e^{a_1/T}-1)^2}$, where a_1, a_2, and a_3 are constants, to demonstrate the specific heat jumps ΔC_{CDW}. The entropy change ΔS_{CDW} across the CDW transition is obtained by integrating the curve under $\Delta C_{CDW}/T$ as a function of T. The transition temperature T_{CDW}, specific heat jumps ΔC_{CDW}, and the entropy change ΔS during warming and cooling the sample (seen in Fig. 7) are listed in Table II. The values of transition temperatures are in good agreement with both the susceptibility and resistivity results.

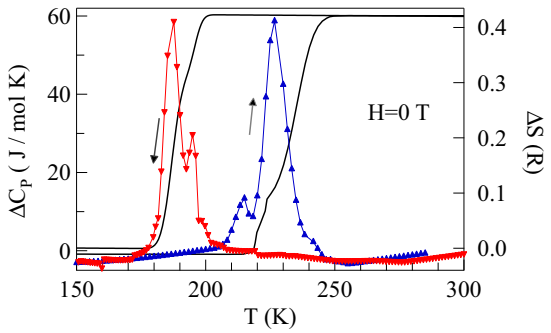

FIG. 7. (Color online) The temperature dependence of excess specific heat ΔC_P vs T (left axis) on both warming (blue triangle) and cooling (red triangle) of $Lu_2Ir_3Si_5$ obtained by subtracting a smooth background from the measured data. Entropy ΔS associated with the transition is estimated after background subtraction, shown in the right axis of the plot.

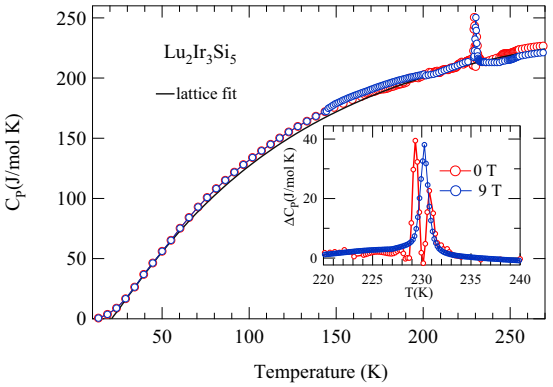

FIG. 8. (Color online) The specific heat of $Lu_2Ir_3Si_5$ in the field of 0 and 9 T while warming the sample from 10 to 270 K. Inset shows the specific heat in a narrow temperature range between 220 and 240 K.

Besides, it is observed that the specific heat anomaly and the entropy change for the $Lu_2Ir_3Si_5$ single crystal are much larger and sharper than that of conventional CDW systems such as $K_{0.3}MoO_3$ (8 J/mol K, 0.18R) [22–24] and $NbSe_3$ ($\sim$9 J/mol K, 0.08R) [25].

The presence of a sharp anomaly in the specific heat data gives the clear evidence of a high electron density and a large amplitude of the periodic lattice distortion accompanying the CDW. Compared to 2H-$TaSe_2$ and 2H-TaS_2 layered compounds [26], this large phonon specific heat anomaly may be due to the presence of an incommensurate CDW phase. According to McMillan's model, proposed for strong CDW systems [27], the first order characteristics of the CDW arises due to considerable phonon softening at the high temperature CDW transition. Besides, the theory proposes that when the coherence length of the CDW state is short, the lattice plays a dominant role in the thermodynamics of the CDW transition with a strong critical behavior.

On the other hand, a large number of soft phonon modes in the transition region contribute substantially to the specific heat and thus a huge specific heat jump is displayed in the $Lu_2Ir_3Si_5$ compound. Similar results have been reported in $Lu_5Ir_4Si_{10}$ [11]. This huge cusp in specific heat data ($\Delta C_{CDW} = 62$ J/mol K) and the pronounced thermal hysteresis, in the warm up and cooling down scans, are the characteristic features expected in a strongly coupled first order CDW transition. The additional peaks observed at 218 and 186 K in the heating and cooling curves, respectively (shown in Fig. 7), indicate the mixture of multiple CDW transition in the compound. One could also observe that an additional (or weaker) specific heat peak is observed at a higher temperature than that of the sharp one in the cooling curve, whereas an opposite trend is observed in the warming curve. This may due to the fact that the system first goes to an incommensurate (IC) state followed by an IC to commensurate (lock-in) transition, as the temperature is lowered from the normal state above the CDW transition. On the other hand, the system undergoes first order multiple CDW transitions and the phases may occur in the order normal state-incommensurate-commensurate either by decreasing or increasing temperature on cooling and warming, respectively. These findings are well consistent with the above mentioned resistivity and susceptibility studies.

TABLE II. The parameters obtained from heat capacity studies (Fig. 7) of $Lu_2Ir_3Si_5$.

	T_{CDW} (K)	Total ΔC_{CDW} (J/mol K)	Total $\Delta S(R)$
Warming curve	218 K		
	232 K	62	0.42
cooling curve	185 K	62	0.42
	198 K		

Figure 8 demonstrates the specific heat of $Lu_2Ir_3Si_5$, taken in PPMS, in the field of 0 and 9 T while warming the sample from 10 to 270 K. By showing the plot, one could analyze the two sets of data (0 and 9 T) originating from the same method, i.e., PPMS station. As we mentioned above, zero field specific heat data show sharp multiple peaks, whereas specific heat with applying a magnetic field of 9 T shows only a sharp peak ($\Delta C_P = 42$ J/mol K) at around 230 K. It might be stressed here that the multiple transitions are suppressed by applying a field of 9 T. The weak anomalies seen at 140 and 195 K in Fig. 8 are probably due to artifacts of the measurements. We do not observe any anomaly at this temperature either in the magnetization or in the resistivity studies.

IV. DISCUSSION

In this section we will discuss the possible origin of multiple CDW transitions observed in $Lu_2Ir_3Si_5$ single crystal. In this context it is worthwhile to recapitulate multiple CDW transitions observed in other materials. The transition metal dichalcogenides 1T -$TaSe_2$ are a well known example of first order multiple CDW transitions and exhibit an incommensurate CDW above 473 K and a commensurate CDW below 473 K. The phases occur in the order normal state-incommensurate-commensurate with decreasing temperature. Similarly, $NbSe_3$, a two-dimensional (2D) layered compound, revealed multiple CDW transitions at 145 and 49 K [28]. In this case, the two CDW would have different wavelengths

and their formation would take place at different temperatures and they are not correlated. The system requires two independent Fermi nesting conditions for the development of two CDW anomalies. Interestingly, multiple CDW transitions are also reported in 3D compounds such as $R_5Ir_4Si_{10}$ (R = rare earth) [10]. In these compounds, the rare-earth atoms forms a chainlike structure along the *c* axis resulting in the formation of a quasi-1D chain. It is observed that in these materials the low temperature purely commensurate CDW phase is achieved via a 1D incommensurate CDW phase transition at high temperatures. This is endorsed by superlattice reflections at various temperatures.

In this paper we describe the sharp first order phase transition in $Lu_2Ir_3Si_5$ with very clear multiple CDW ordering with respect to resistivity, susceptibility, and specific heat measurement. In order to clarify the presence of multiple charge-density-wave transitions in $Lu_2Ir_3Si_5$, it is important to point out the quality of the single crystal as well as the details of the measurements. The single-crystalline nature of the samples was verified using a Laue diffraction technique. The well-defined spots observed in the Laue diffraction pattern of $Lu_2Ir_3Si_5$ along [100], [010], and [001] directions confirm the absence of multiple domains of the grown crystal. In addition, the crystal structure studies on powder XRD at 300 K, EDAX and EPMA analysis at various positions of the crystal clearly reveals the purity of single phase and homogeneity of the compound as well. Hence it is very clear that appearance of only two inflections, consistently appearing in a large number of crystals, arise not from the pinning or nucleation of different domains on facets or mosaics within the single crystal. TEM images (Fig. 4) also do not reveal any such defects. We agree that the other types of strains arising to various defects like dislocations, etc. may be present and quantifying them is not easy. Efforts have been made to reduce such defects by annealing the sample for a long period of 15 days. Even bulk specific heat measurements with only two jumps in different single crystals dismiss the idea of defect induced multiple CDW transitions. Moreover, our result is in conjunction with the previous reports by Lee *et al.* [17]. In accordance with their TEM study, a structural phase transition temperature was clearly observed along with the CDW superlattice formation. It is also noted that the system undergoes the incommensurate and commensurate CDW transition. It is very unlikely that both the incommensurate and commensurate CDW transitions occur at the same temperature. Hence two such transitions are an expected feature. Moreover, our preliminary analysis of TEM measurement in $Lu_2Ir_3Si_5$ along the [100] axis also reveals that the system undergoes orthorhombic to orthorhombic transition by distorting the lattice parameters below 150 K.

Adding to the fact that, by looking at the crystal structure of $Lu_2Ir_3Si_5$ (Fig. 3), it can be safely assumed that the CDW anomalies are related to the quasi-1D chain of Lu atoms along the *c* axis. Hence we speculate that this Lu chain of atoms might be rearranging themselves twice via commensurate/incommensurate modes, resulting in an appearance of multiple CDW phases. Such multiple transitions is favorable to be observed along *a* and *c* axes as this compound has the zigzag chain of Lu atoms spread over the *bc* plane. Both resistivity and susceptibility results corroborate the above inference. Interestingly, the susceptibility data along the *c* axis show an upward jump across the CDW ordering, whereas it shows a drop in susceptibility along the *a* and *b* axes. From the jump in the susceptibility and the specific heat anomaly, we have estimated ∼35% reduction in the electronic density of states (DOS) at the Fermi surface along the *a* axis, whereas it shows a ∼60% drop along the *b* axis. In contrast, the *c* axis shows ∼25% enhancement in DOS at the Fermi surface. The upward jump across the CDW ordering in susceptibility data is exceptional in a conventional CDW system. According to crystal structure, the zigzag chain of the Lu atom along the *c* axis is strongly coupled with the *b* axis through the Ir1 atom. Hence, it could be possible here that the additional modulation of the DOS is restored at the Fermi level, whereas in the other two axes additional DOS is removed at the Fermi level. However, it is only a conjecture. More investigations, preferably band structure calculations, are needed for complete understanding of this enhancement of magnetization at the CDW region and to determine the possible nesting and gaping of the FS rather than an expected diamagnetic drop here.

Furthermore, the specific heat measurement performed in PPMS, in an applied magnetic field of 9 T, shows only a single peak at 232 K rather than multiple CDW anomalies. Since the specific heat measurement in the PPMS system is not an adiabatic measurement, it may average out the transition that causes the disappearance of weak anomaly. At the same time, it also highlights the possibility of self-critical phenomena in this CDW system. Generally, self-critical phenomena in CDW systems are related to the suppression of the anomaly with applied magnetic field. Nevertheless, a detailed microscopic description of the properties of this solid has to be required for further understandings.

V. CONCLUSION

We have investigated the physical properties of a $Lu_2Ir_3Si_5$ single crystal using magnetic susceptibility, electrical resistivity, specific heat, and TEM measurements. It found that the compound exhibits first order multiple CDW transitions associated with a large thermal hysteresis of about 50 K with respect to transport and thermal experiments. Interestingly, TEM results reveal that the system undergoes orthorhombic to orthorhombic transition by distorting the lattice constants along *b* and *c* axes below the CDW ordering temperature (below 150 K). Besides, the giant excess of specific heat $\Delta C_P/C_P \sim 26\%$ and the huge specific heat jump (62 J/mol K) further support the strong coupling first order CDW scenario. Definite conclusion of aforesaid scenarios need further experimentation on $Lu_2Ir_3Si_5$, concerning structural fluctuation and lattice softening (inelastic neutron scattering). In addition, synchrotron x-ray study of the system is to be performed to determine *q* vectors for the CDW transition.

ACKNOWLEDGMENTS

N.S.S. thanks Professor A. K. Grover, TIFR Mumbai, for his various kind support throughout the current research work. N.S.S. is also grateful to Bhanu Joshi and Om Prakash for their help in various ways. C.V.T. would like to acknowledge the

Department of Science and Technology for the partial support through Project No. IR/S2/PV-10/2006. S.B. and P.R. would like to acknowledge Jayesh B. Parmar for his help during TEM sample preparation.

[1] R. E. Peierls, *Quantum Theory of Solids* (Oxford University Press, New York, 1955).
[2] G. Gruner, *Density Waves in Solids* (Addison-Wesley, Reading, MA, 1994).
[3] L. Degiorgi, B. Alavi, G. Mihaly, and G. Gruner, Phys. Rev. B **44**, 7808 (1991).
[4] S. Sridhar, D. Reagor, and G. Gruner, Phys. Rev. Lett. **55**, 1196 (1985).
[5] T. Giamarchi, S. Biermann, A. Georges, and A. Lichtenstein, J. Phys. IV (France) **114**, 23 (2004).
[6] A. Schwartz, M. Dressel, G. Gruner, V. Vescoli, L. Degiorgi, and T. Giamarchi, Phys. Rev. B **58**, 1261 (1998).
[7] Y. Singh, D. Pal and S. Ramakrishnan, Phys. Rev. B **70**, 064403 (2004).
[8] H. D. Yang, P. Klavins, and R. N. Shelton, Phys. Rev. B **43**, 7688 (1991).
[9] K. Ghosh, S. Ramakrishnan, and G. Chandra, Phys. Rev. B **48**, 4152 (1993).
[10] S. van Smaalen, M. Shaz, L. Palatinus, P. Daniels, F. Galli, G. J. Nieuwenhuys, and J. A. Mydosh, Phys. Rev. B **69**, 014103 (2004).
[11] B. Becker, N. G. Patil, S. Ramakrishnan, A. A. Menovsky, G. J. Nieuwenhuys, J. A. Mydosh, M. Kohgi, and K. Iwasa, Phys. Rev. B **59**, 7266 (1999).
[12] Y. Feng, J. Wang, R. Jaramillo, J. V. Wezel, S. Haravifard, G. Srajer, Y. Liu, Z.-A. Xu, P. B. Littlewood, and T. F. Rosenbaum, Proc. Natl. Acad. Sci. USA **109**, 7224 (2012).
[13] J. C. Petersen, S. Kaiser, N. Dean, A. Simoncig, H. Y. Liu, A. L. Cavalieri, C. Cacho, I. C. E. Turcu, E. Springate, F. Frassetto, L. Poletto, S. S. Dhesi, H. Berger, and A. Cavalleri, Phy. Rev. Lett. **107**, 177402 (2011).
[14] B. Mansart, M. J. G. Cottet, T. J. Penfold, S. B. Dugdale, R. Tediosi, M. Chergui, and F. Carbone, PNAS **109**, 5603 (2012).
[15] Y. Singh, D. Pal, S. Ramakrishnan, A. M. Awasthi, and S. K. Malik, Phys. Rev. B **71**, 045109 (2005).
[16] Y. K. Kuo and K. M. Sivakumar, T. H. Su, and C. S. Lue, Phys. Rev. B **74**, 045115 (2006).
[17] M. H. Lee, C. H. Chen, M.-W. Chu, C. S. Lue, and Y. K. Kuo, Phys. Rev. B **83**, 155121 (2011).
[18] N. S. Sangeetha, A. Thamizhavel, C. V. Tomy, S. Basu, A. M. Awasthi, S. Ramakrishnan, and D. Pal, Phys. Rev. B **86**, 024524 (2012).
[19] J. Rodriguez-Carvajal, Phys. B: Condens. Matter **192**, 55 (1993).
[20] T. Das, S. Bhattacharyya, B. P. Joshi, A. Thamizhavel, and S. Ramakrishnan, Direct evidence of intercalation in a topological insulator turned superconductor, Mater. Lett. **93**, 370 (2013).
[21] F. Galli, S. Ramakrishnan, T. Taniguchi, G. J. Nieuwenhuys, J. A. Mydosh, S. Geupel, J. Lüdecke, and S. vanSmaalen, Phys. Rev. Lett. **85**, 158 (2000).
[22] J. W. Brill, M. Chung, Y.-K. Kuo, X. Zhan, E. Figueroa, and G. Mozurkewich, Phys. Rev. Lett. **74**, 1182 (1995).
[23] R. S. Kwok and S. E. Brown, Phys. Rev. Lett. **63**, 895 (1989).
[24] R. S. Kwok and G. Gruner, S. E. Brown, Phys. Rev. Lett. **65**, 365 (1990).
[25] S. Tomić, K. Biljaković, D. Djurek, J. R. Cooper, P. Monceau, and A. Meerschaut, Solid State Commun. **38**, 109 (1981).
[26] R. A. Craven and S. F. Meyer, Phys. Rev. B **16**, 4583 (1977).
[27] W. L. McMillan, Phys. Rev. B **12**, 1187 (1975).
[28] J. L. Hodeau, M. Marezio, C. Roucau, R. Ayroles, A. Meerschaut, J. Rouxel, and P. Monceau, J. Phys. C **11**, 4117 (1978).